ACS APPLIED MATERIALS & INTERFACES

www.acsami.org

Research Article

The Surface Energy of Hydrogenated and Fluorinated Graphene

James Carpenter,[⊥] Hyunchul Kim,[⊥] Jules Suarez, Arend van der Zande,* and Nenad Miljkovic*

Cite This: *ACS Appl. Mater. Interfaces* 2023, 15, 2429−2436

Read Online

ACCESS | Metrics & More | Article Recommendations | Supporting Information

ABSTRACT: The surface energy of graphene and its chemical derivatives governs fundamental interfacial interactions like molecular assembly, wetting, and doping. However, quantifying the surface energy of supported two-dimensional (2D) materials, such as graphene, is difficult because (1) they are so thin that electrostatic interactions emanating from the underlying substrate are not completely screened, (2) the contribution from the monolayer is sensitive to its exact chemical state, and (3) the adsorption of airborne contaminants, as well as contaminants introduced during transfer processing, screens the electrostatic interactions from the monolayer and underlying substrate, changing the determined surface energy. Here, we determine the polar and dispersive surface energy of bare, fluorinated, and hydrogenated graphene through contact angle measurements with water and diiodomethane. We accounted for many contributing factors, including substrate surface energies and combating adsorption of airborne contaminants. Hydrogenating graphene raises its polar surface energy with little effect on its dispersive surface energy. Fluorinating graphene lowers its dispersive surface energy with a substrate-dependent effect on its polar surface energy. These results unravel how changing the chemical structure of graphene modifies its surface energy, with applications for hybrid nanomaterials, bioadhesion, biosensing, and thin-film assembly.

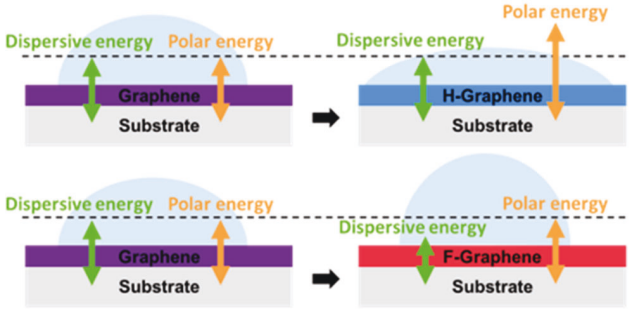

KEYWORDS: *graphene, wettability, surface energy, chemical functionalization, 2D materials*

1. INTRODUCTION

Understanding of complex nanoscale surface−liquid interactions is critical to realizing applications in diverse fields including biosensing,[1−3] molecular assembly,[4] and energy transport.[5] One emerging area is understanding the surface−liquid interactions in two-dimensional (2D) materials, whose atomic-scale thickness and diverse electronic transport mechanisms open up new fundamental properties, opportunities, and challenges. For example, 2D materials like graphene are both highly sensitive to changes in their environment and highly deformable, making them excellent candidates for materials having reconfigurable surface properties,[6] ultrasensitive disease detection,[1,7] and that can be interfaced with cells.[8,9] For all of these applications, the surface energy of graphene is a key parameter governing processes such as liquid wettability, protein adsorption,[10−12] and cell adhesion and growth,[13,14] making it important to characterize. Moreover, the van der Waals surface of graphene is chemically inert, making it difficult to selectively design the surface interactions needed for many of the applications.

A promising strategy is to leverage vapor phase chemical functionalization of graphene with hydrogen and fluorine, which modifies its chemical structure to produce hydrogenated graphene (HGr)[15−17] and fluorinated graphene (FGr), respectively.[18−20] Compared with bare graphene, these chemical functionalizations strongly modify wettability[13,17] and surface friction,[21] enhance cell adhesion,[13,17] and encourage thin-film growth via atomic layer deposition (ALD) or chemical bath deposition.[22−24] Moreover, functionalized graphene can be patterned[17,25] and integrated into devices,[26,27] opening up the possibilities of guiding wettability and site-selective adsorption.

Critical to the rational design in these applications is quantifying the changes in surface energy for different kinds of graphene functionalization. Surface energy is a property dominant in many molecular and liquid interfacial interactions. Nevertheless, despite numerous studies, disagreements about the surface energy of bare graphene remain for at least three reasons. First, the surface energy of supported graphene is not a fixed value as it is affected by its supporting substrate, leading to so-called wetting translucency.[28−32] Second, transferring graphene from its growth substrate to a target substrate typically involves several processing steps that can contaminate its surface with various ions and residues, affecting the intrinsic surface interactions. Finally, the adsorption of volatile organic

Received: October 11, 2022
Accepted: December 1, 2022
Published: December 23, 2022

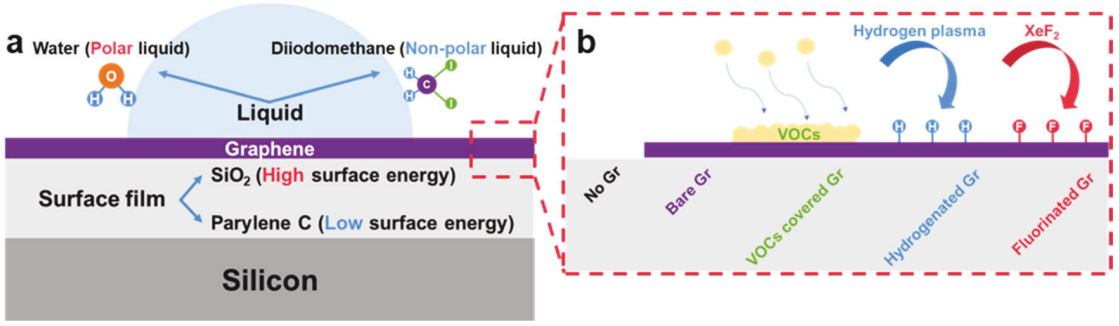

Figure 1. (a) Schematic showing the various parameters under study to probe the affect they have on the determined surface energy of graphene. We used water and diiodomethane as polar and nonpolar probe liquids, respectively, for contact angle measurements and subsequent surface energy analysis, as well as SiO_2 and Parylene C as high and low surface energy supporting substrates, respectively, for (b) the various graphene functionalizations tested (i.e., bare graphene, VOC-Gr, HGr, and FGr).

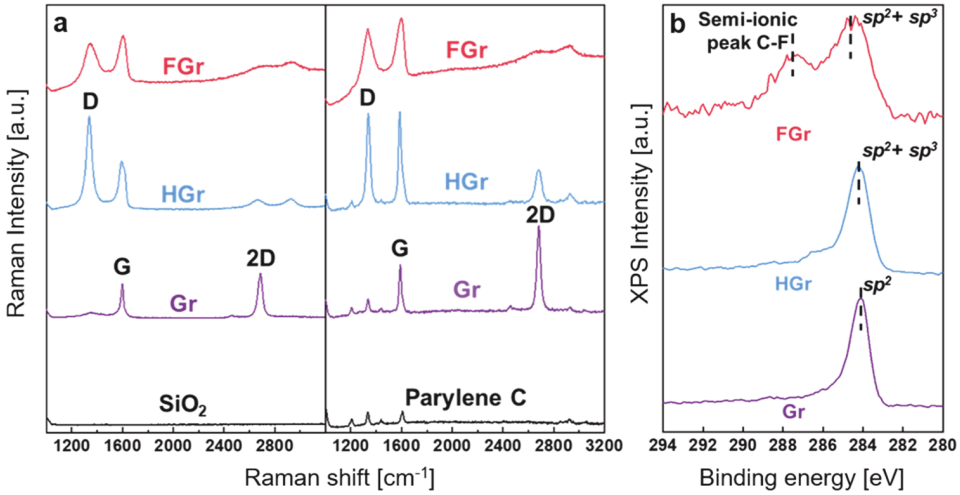

Figure 2. (a) Raman spectra of the SiO_2 substrate, as well as bare graphene, HGr, and FGr supported by SiO_2 (left) and the same for ParC (right). (b) XPS spectra of the C 1s core-level spectra comparing bare graphene, HGr, and FGr.

compounds onto a surface in ambient conditions is a confounding factor across all of interfacial science.[33−37] Volatile organic compounds (VOC) are compounds that have a high vapor pressure and low water solubility. These VOC are emitted from a wide range of human-made chemicals and can adsorb to surfaces and screen intrinsic surface interactions.[33] In the case of atomically thin 2D materials, the adsorbed layers can be many times thicker than the material itself, preventing accurate measurements.[38−41] Most studies do not simultaneously account for all of the aforementioned challenges, leading to contradictory results routinely being reported on the surface energy and wettability of supported bare graphene.[42−46] In the case of FGr and HGr, it is unclear how the added out-of-plane bond affects the surface energy of supported graphene and what contribution, if any, the substrate will have through wetting translucency. Moreover, the relative strength and interdependence of these different phenomena are currently unknown. This knowledge is necessary to rationally design functionalized graphene for a variety of applications, including the ones discussed thus far.

In this study, as shown schematically in Figure 1, we characterized the wettability and corresponding polar and dispersive surface energies of supported monolayer graphene and its functionalized counterparts (FGr and HGr). To ensure consistent results, we used a transfer process that limited contamination and then systematically examined the relative surface energy contributions from the chemical functionalization, adsorption of VOC, and the supporting substrate. Using the dispersive and polar surface energy of bare graphene supported by SiO_2 and Parylene C (ParC) as references, our results show that hydrogenating graphene raises its polar surface energy with little effect on its dispersive surface energy. Fluorinating graphene lowers its dispersive surface energy and has a substrate-dependent effect on its polar surface energy. The polar surface energy of FGr supported by SiO_2 is nearly the same as that of bare graphene supported by SiO_2. However, the polar surface energy of FGr supported by Parylene C (the tested supporting substrate with lower polar surface energy) is lower than the polar surface energy of bare graphene supported by Parylene C. The adsorption of VOC lowers the polar surface energy of bare graphene. Meanwhile, the polar surface energy of all graphene types tested is higher on SiO_2, the higher polar surface energy supporting substrate tested. The results reported here can be used to rationally design the surface energy of graphene and other 2D materials for applications in bioadhesion, biosensing, and thin-film assembly.

2. METHODS

To determine the polar and dispersive surface energies of each sample, we made contact angle measurements with a micro-goniometer using polar and nonpolar probe fluids, and then applied

https://doi.org/10.1021/acsami.2c18329
ACS Appl. Mater. Interfaces 2023, 15, 2429−2436

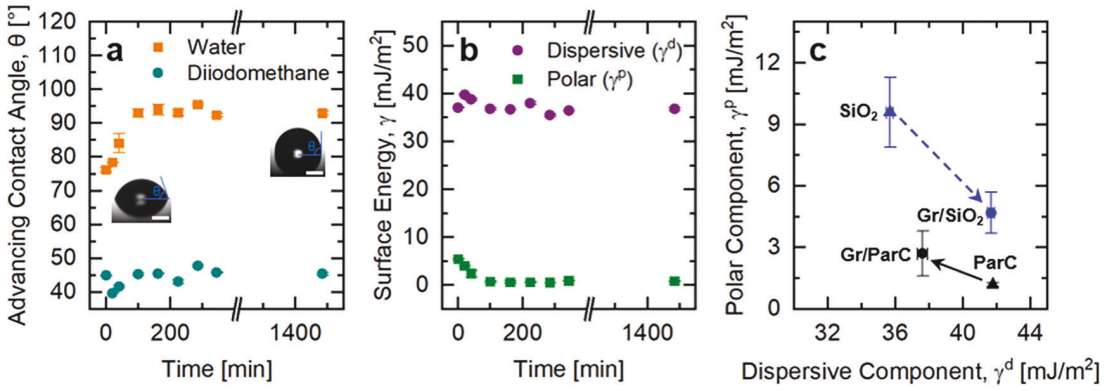

Figure 3. (a) Apparent advancing contact angle of water (orange squares) and diiodomethane (teal circles) as a function of time on bare graphene supported by SiO_2. Insets: optical images illustrating the contact angle at two different times (0 min and 1480 min). The scale bar is 200 μm. Each data point represents the average and standard error from three to five sequential contact angle measurements with three to five distinct droplets for each probe fluid on the same region. (b) Corresponding dispersive (purple) and polar (green) surface energy components as a function of time of bare graphene on SiO_2 extracted from data plotted in (a). (c) Comparison between the dispersive and polar surface energy components of SiO_2 and graphene on SiO_2 (blue) as well as Parylene C and graphene on Parylene C (black). All measurements in (c) are taken within 5 min of air exposure to minimize the impact of VOC contamination and probe intrinsic substrate and graphene surface properties. The uncertainties are shown in (a−c) and are frequently smaller than the symbol size.

Fowkes' theory to extract the surface energies (see Sections S1 and S2, Supporting Information).[47,48] We used deionized water (CAS: 7732-18-5, Thermo Scientific) as the polar probe fluid and diiodomethane (CAS: 75-11-6, Sigma-Aldrich) as our nonpolar probe fluid. We examined the influence of the supporting substrate on the surface energy of graphene by transferring monolayer graphene to substrates with different surface energy. Supporting Information, Section S3 provides descriptions of the detailed methods used for substrate preparation, graphene transfer, and cleaning. We used polished silicon wafers having an annealed 285 nm thick silicon dioxide (SiO_2) layer (thermally oxidized, Nova Electronic Materials) as our higher surface energy supporting substrate. We deposited 200 nm of Parylene C (ParC) onto the SiO_2 wafers, which served as our lower surface energy supporting substrate, using chemical vapor deposition (CVD, SCS Labcoter 2, Specialty Coating Systems).

As shown in Figure 1b, we systematically compared the effect of each different chemical functionalization on the polar and dispersive components of the surface energy of graphene. Specifically, we compared the cases of no graphene (bare substrates), bare graphene (Gr), graphene after VOC adsorption (VOC-Gr), hydrogenated graphene (HGr), and fluorinated graphene (FGr). Supporting Information, Sections S4 and S5 provide detailed methods used to conduct functionalization and sample storage. Briefly, to make the samples, we transferred chemical vapor deposition (CVD) grown graphene onto each substrate. We used established dry transfer techniques, which minimize doping and residue at the graphene-substrate interface.[49,50] Figure S1 shows optical and atomic force microscopy topography images of the transferred graphene, confirming that the graphene was clean with minimal particles or damage which might affect measurements. Finally, the graphene was annealed in a reducing atmosphere. To systematically study and minimize the effects of VOC adsorption, we used a pressurized inert gas vessel filled with adsorbents to house and transport samples until measurement or functionalization. Finally, we used established processes to functionalize the graphene by leaving the sample in ambient conditions for VOC adsorption,[38−41] exposure to indirect hydrogen plasma for hydrogenation,[15,17,51] or exposure to XeF_2 gas for fluorination.[18,52]

To confirm sample quality, functionalization, and chemical bonding we used Raman spectroscopy and X-ray photoelectron spectroscopy (XPS) (see Section S6, Supporting Information). Figure 2a shows the Raman spectra of the substrates, bare graphene, HGr, and FGr on SiO_2 and ParC. The bare graphene on SiO_2 sample showed the G and 2D peaks at 1596 ± 1 and 2684 ± 2 cm^{-1}, respectively,[53,54] with a ~1.3 intensity ratio. The D-peak at 1360 ± 1 cm^{-1} is less than 0.16 of the intensity of the G-peak, indicating a low but nonzero defect density. These values are comparable to those for annealed CVD-grown monolayer graphene.[55] In comparison, the HGr and FGr spectra show a suppressed 2D peak and increased D-peak due to sp^3 bond formation with the hydrogen and fluorine, respectively.[21] The spectra of the functionalized graphene on the ParC substrate show similar trends.

Figure 2b shows the XPS spectra of bare, HGr, and FGr on SiO_2. Bare graphene exhibits the sp^2 bond peak in the C 1s core-level spectra centered at 284.14 ± 0.02 eV. For HGr, this peak is broadened and one more peak emerges at 285.42 ± 0.15 eV, indicating the conversion of sp^2 to C−H bonds.[56] For FGr, another peak emerges at 287.18 ± 0.03 eV, indicating the formation of semi-ionic C−F bonds.[20] Thus, both the Raman and XPS spectra confirm the hydrogenation and fluorination of graphene.

3. RESULTS

Next, we examine the effect that the adsorption of airborne contaminants has on the contact angles measured on the samples. A challenge in interpreting the measured water contact angle on graphene and other surfaces is the effect of adsorption of VOC under ambient measurement conditions, which screen the true surface interactions, and can lead to a wide range of measured contact angles from 37 to 90°.[39,57] To examine the effects of VOC adsorption, as plotted in Figure 3a, we exposed bare graphene supported by SiO_2 to ambient lab conditions for approximately 24 h while periodically performing advancing contact angle measurements with both water and diiodomethane (see Section S1, Supporting Information). We measured the advancing contact angle, as opposed to the receding or so-called static contact angle because it is far less sensitive to surface chemical heterogeneities and topographical features.[33] Between measurements, the sample was placed top-up in a petri dish with no lid in a laboratory located in Urbana, IL.

Figure 3a plots the advancing contact angle as a function of ambient exposure time for water (teal circles) and diiodomethane (orange squares) probe liquids on bare graphene supported by SiO_2. Each data point represents the average and standard error from three to five sequential contact angle measurements with distinct droplets for each probe fluid on the same region. The diiodomethane contact angle on

https://doi.org/10.1021/acsami.2c18329
ACS Appl. Mater. Interfaces 2023, 15, 2429−2436

Table 1. Summary of the Water and Diiodomethane Advancing Contact Angle (ACA) Measurements with Corresponding Dispersive and Polar Surface Energy Values for All Samples Tested

substrate	surface	water ACA (deg)	diiodomethane ACA (deg)	γ^d (mJ/m^2)	γ^p (mJ/m^2)
SiO_2		68.1 ± 2.6	47.5 ± 0.7	35.7 ± 0.2	9.6 ± 1.7
	Gr	75.4 ± 1.5	35.8 ± 0.6	41.7 ± 0.2	4.7 ± 1.0
	VOC-Gr[a]	92.9 ± 0.6	45.4 ± 0.5	36.8 ± 0.3	0.8 ± 0.1
	HGr	39.3 ± 0.3	36.4 ± 1.4	41.4 ± 0.3	23.4 ± 0.3
	FGr	84.6 ± 0.6	64.6 ± 2.2	25.9 ± 0.3	5.0 ± 0.4
Parylene C		87.6 ± 0.1	35.6 ± 0.2	41.7 ± 0.0	1.2 ± 0.1
	Gr	83.6 ± 2.0	43.9 ± 1.4	37.6 ± 0.3	2.7 ± 1.1
	VOC-Gr[a]	96.8 ± 0.3	48.1 ± 1.1	35.3 ± 0.6	0.37 ± 0.01
	HGr	46.2 ± 3.1	37.3 ± 1.6	40.9 ± 0.3	19.7 ± 2.3
	FGr	103.7 ± 0.7	71.1 ± 0.6	22.3 ± 0.0	0.6 ± 0.2

[a]Measurements obtained for VOC-Gr supported by SiO_2 and Gr supported by SiO_2 were obtained from different samples. The same is true for VOC-Gr supported by Parylene C and Gr supported by Parylene C.

graphene fluctuates between 40 and 45° for the duration of the experiment. In contrast, the advancing water droplet contact angle on graphene increases from an initial value of 76.2 ± 0.6 to 92.9 ± 0.6° in the first 100 min, then levels off. We attribute the small fluctuation of the contact angle measurements over time to the heterogeneity of the samples and the inability to perform measurements at the exact same location consistently. Supporting Information, Figure S2 confirms that the trends are reproducible on a second sample. Figure 3b plots the corresponding change in the polar and dispersive surface energy components versus ambient exposure time. We extract the separate components by inserting the water and diiodomethane contact angles into Fowkes' theory (see Section S2, Supporting Information). Over time, the change in dispersive surface energy of graphene on SiO_2 reduces to less than the error between measurements, only decreasing from γ^d = 37.1 ± 0.1 mJ/m^2 to γ^d = 36.8 ± 0.3 mJ/m^2. In contrast, the polar surface energy decreases significantly, from γ^p = 5.4 ± 0.2 mJ/m^2 to γ^p = 0.8 ± 0.1 mJ/m^2.

The measurements show that the water contact angle is dictated by the adsorption of VOC for samples exposed to air for over an hour, regardless of any previous treatment. To minimize the influence of VOC adsorption and to enable the measurement of intrinsic properties, we built a custom airtight vessel (Supporting Information, Figure S3), filled it with adsorbents (HS-600, Hydrosil International) tailored for a wide range of VOC, then pressurized it with inert argon gas (99.999% purity). We used the vessel to store and transport samples between fabrication and measurement locations. Supporting Information, Table S1 shows that storing samples in the vessel effectively minimizes the adsorption of VOC. This experimental measure was especially necessary for the chemically functionalized HGr and FGr samples as traditional methods of cleaning bare graphene, such as annealing or UV exposure, degrade the functionalization.[15,18,52] For all subsequent data, the samples were exposed to ambient conditions for <5 min between removal from the annealing system and contact angle measurements.

Figure 3c compares the surface energy of characteristic substrates with and without bare graphene before VOC adsorption. To minimize the potential influence of different sample processing conditions, we measured regions with and without the graphene on the same substrates. Table 1 summarizes the measured contact angles and extracted surface energies for every measured combination. The dispersive surface energy of SiO_2 increased by 17% with the addition of bare graphene. The polar surface energy of SiO_2 decreased by 51% with the addition of bare graphene. Conversely, the dispersive surface energy on ParC decreased by 10% with the addition of bare graphene. The polar surface energy of ParC increased by 125% with the addition of bare graphene.

Figure 4 compares how different chemical functionalizations influence the resulting surface energy of graphene supported by

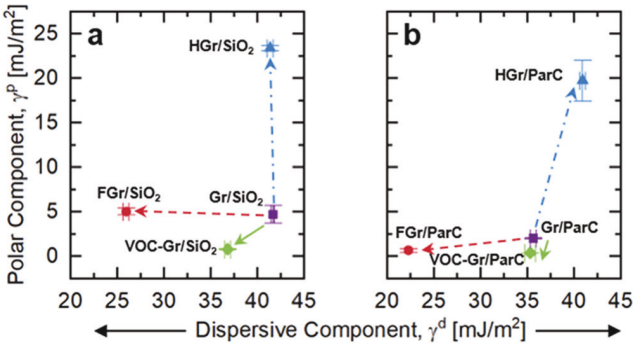

Figure 4. Plots of polar versus dispersive components of surface energies of bare graphene (purple), VOC-contaminated graphene (green), fluorinated graphene (red), and hydrogenated graphene (blue) supported by (a) SiO_2 and (b) Parylene C (ParC). Arrows show the relative change in surface energies of functionalized versus bare graphene. Each data point is the average calculated surface energy and standard error obtained from three to five water and diiodomethane contact angle measurements on the sample. The arrows indicate the change compared with bare graphene on each substrate.

SiO_2 (Figure 4a) and ParC (Figure 4b). Table 1 lists the corresponding contact angles and surface energies for each substrate. Each functionalization has a unique effect on surface energy. Adsorption of VOC on graphene supported by SiO_2 and ParC reduces the dispersive surface energy by 12 and 6%, respectively, while more significantly reducing the polar surface energy by 83 and 86%, respectively. Fluorination of graphene (FGr) supported by SiO_2 and ParC significantly reduces the dispersive surface energy by 38 and 41%, respectively. However, fluorination leads to opposite behavior for polar surface energy on the two substrates. On SiO_2, fluorination raises the polar surface energy by 6% while on ParC fluorination lowers the polar surface energy by 78%. Hydrogenation of graphene (HGr) leads to opposite behavior in the change of dispersive surface energy on the two substrates. On

https://doi.org/10.1021/acsami.2c18329
ACS Appl. Mater. Interfaces 2023, 15, 2429−2436

SiO_2, hydrogenation slightly lowers the dispersive surface energy by 1%, while on ParC hydrogenation raises the dispersive surface energy by 9%. Finally, hydrogenation significantly increases the polar surface energy by 398 and 630% on SiO_2 and ParC, respectively.

4. DISCUSSION

To understand the change of the polar and dispersive surface energy of graphene due to VOC adsorption and each type of chemical functionalization, we need to understand how the interconnected roles of nanoscale screening, charge transfer between graphene and its supporting substrates, and dipoles produced by molecular bonding influence each surface energy type. Dispersive interactions originate from temporary fluctuations in the electron density surrounding an atom or molecule.[58] Dispersive interactions are not site-specific as they exist between all matter. The strength of these interactions scales with the polarizability of the atoms/molecules involved, and are not additive; that is, the interaction between two bodies is affected by the presence of other bodies nearby. Nondispersive, or polar, interactions arise from Coulombic interactions between atoms and molecules, and the polar surface energy scales with the strength of these polar interactions. Typical examples include dipole−dipole (Keesom), dipole-induced dipole (Debye), hydrogen-bonding, and pi−hydrogen interactions. Polar interactions are site-specific and can be present or absent depending on the system under consideration.[58,59]

Our results show differences in the polar and dispersive surface energy of bare graphene supported by SiO_2 and ParC. The polar surface energy of graphene supported by SiO_2 is higher than the polar surface energy of graphene supported by ParC (Figure 3c), which suggests that the higher the polar surface energy of the substrate, the higher the polar surface energy of the supported graphene. This result is consistent with others indicating that graphene is wetting translucent to its supporting substrate.[28−30] To validate these results, we compare them with other studies. Table S2 shows that the surface energy of bare graphene varies significantly as a function of the supporting substrate, ranging from $0.2 \leq \gamma^p \leq 14.4$ mJ/m^2 for the polar surface energy and $14.7 \leq \gamma^d \leq 47.8$ mJ/m^2 for the dispersive surface energy. Moreover, even on the same substrate, there is a wide range of reported values for the surface energy of bare graphene supported by SiO_2. The polar and dispersive surface energy of bare graphene supported by SiO_2 ranges from $1.5 \leq \gamma^p \leq 5.3$ mJ/m^2 to $14.7 \leq \gamma^d \leq 35.7$ mJ/m^2, respectively. Given this variability in reported values, more systematic measures are required for analyzing the surface energy of graphene. Our study implemented many measures to ensure reproducible, high-fidelity results, including dry transfer of the graphene, post-annealing in a reducing atmosphere, and storing samples in a pressurized inert gas. Our results show that, while there are observable shifts in both the polar and dispersive surface energies, the relative change in the polar surface energy compared with the initial value is much larger than the shift in the dispersive energy, and more easily interpretable.

In the case of VOC adsorption, the nonadditive nature of dispersive interactions makes it challenging to identify the cause of relatively small changes in dispersive surface energy, especially considering the speed of adsorption and the chemical similarity between graphene and VOCs.[33] Despite our best efforts, preventing VOC adsorption is practically impossible, even under vacuum conditions.[37] Thus, a few layers of VOCs can quickly adsorb and alter the dispersive interaction between graphene and our probe liquid. This is evident in Figure 3a,b, where the diiodomethane contact angle, and corresponding dispersive surface energy, changes little with time, potentially indicating that the determined dispersive surface energy is being driven by VOC adsorption. Moreover, the polar surface energy decreases to zero over time due to increased screening from VOC layers, which are mostly composed of light, short-chained, nonpolar hydrocarbons.[33,34,60] As more VOC layers adsorb with time, the polar interaction potential emanating from the surface/substrate is screened out, causing the water contact angle to rise and polar surface energy to fall. The rise in hydrophobicity resulting from VOC adsorption has been observed in other labs with presumably distinct VOC adsorption conditions, indicating a universality to the process and its effect on measured water contact angles.[39,40]

Both types of chemically functionalized graphene modify the in-plane sp^2 bonds of pristine graphene to form out-of-plane sp^3 bonds, which modify its electronic structure and induce out-of-plane dipole moments. First, the sp^3 bonds open a bandgap in the fluorinated/hydrogenated graphene and raise the resistivity from ∼1 kΩ in pristine graphene to ∼10 GΩ in functionalized graphene.[21] Our results indicate that the change in resistivity does not dominate the change in surface energies or else both functionalization types would show similar behavior, opposite of what is observed. Additionally, both the C−F bonds and C−H bonds induce an out-of-plane dipole moment compared with bare graphene,[61,62] which contribute to the change in surface energies of HGr and FGr. The low polarizability of fluorine weakens dispersive interactions.[63] As a result, as we observe, the dispersive surface energy of FGr is smaller than that of bare graphene and HGr. The C−F bond is polar and thus generates a dipole. Therefore, one would expect FGr to have a substantially higher polar surface energy than bare graphene supported by either substrate. Nevertheless, we do not observe a significant increase in the polar surface energy of FGr supported by either substrate. This lower-than-expected polar surface energy of FGr is well documented in other fluorocarbons, a phenomenon known as "polar" hydrophobicity.[62,64,65] The reason in these other cases is that the C−F surface dipoles generate a short-range electric field that decays within the core repulsion zone of the surface. As a result, molecules in liquids do not get close enough to the surface to strongly interact with the strong dipole moment of the C−F bond, leading to a polar surface energy that is lower than expected. This polar hydrophobicity interpretation is consistent with the polar surface energy we determined in this study for FGr supported by SiO_2 and ParC.

The surface energy of all of the graphene samples tested (Gr, FGr, HGr, and VOC-Gr) is translucent to the supporting substrate as the polar surface energy for all graphene samples is higher on SiO_2, the more polar substrate. Since FGr has an inherently low polar surface energy, we attribute the similar polar surface energy of FGr/SiO_2 and Gr/SiO_2 to translucency to the supporting substrate. In contrast, we observe a decrease in the polar surface energy of FGr/ParC compared to Gr/ParC. Since the polar surface energy of ParC is low, it is not transmitted through the graphene films, thus allowing the inherent hydrophobicity of FGr to dominate, resulting in lower polar surface energy for FGr supported by ParC.[28,62]

https://doi.org/10.1021/acsami.2c18329
ACS Appl. Mater. Interfaces 2023, 15, 2429−2436

For HGr, the nonadditive nature of dispersive interactions makes it challenging to identify the cause of relatively small changes in dispersive surface energy, especially considering the chemical similarity between HGr and VOC.[33] The cause for the large increase in the polar surface energy of HGr is harder to identify. The dipole generated by the C−H bond is weak, so it is unlikely to be the main contributor. Supporting substrates with high polar surface energy are known to dope graphene, indicating a charge transfer from graphene to substrate.[44] Thus, it is possible that this charge transfer leaves the top side of graphene with a partial positive charge that can then interact strongly with the dipole of water molecules, raising the polar surface energy and lowering the water contact angle. However, we would expect the charge transfer from graphene to substrate to scale with the polar surface energy of the substrate. Nevertheless, we observe a similar increase in polar surface energy for HGr/SiO_2 and HGr/ParC of 18.7 ± 1.3 and 17.0 ± 3.4 mJ/m^2, respectively, in comparison to Gr/SiO_2 and Gr/ParC, even though the SiO_2 substrate has a polar surface energy 800% larger than that of ParC. The final possible contributor is that the hydrogen plasma used to hydrogenate graphene is activating the substrate. Graphene is known to be permeable to hydrogen ions[66,67] and molecules.[68] Hydrogen ions could also pass through defects produced during the transfer process or imperfect adhesion between the graphene layer and its supporting substrate. Once under the graphene layer, the ions can react to form polar functional groups on the substrate (OH for SiO_2 and HCl for Parylene C), raising the surface energy of HGr through the effect of translucency. The lack of control over the proton permeation or intercalation processes leaves us unable to experimentally distinguish which is the dominant mechanism. While our measurements do not allow us to de-convolve these different possibilities, they set up a framework that could be resolved through atomistic simulations.

5. CONCLUSIONS

In summary, we explored the polar and dispersive surface energy of bare, physically functionalized (VOC-covered), and chemically functionalized (hydrogenated and fluorinated) graphene on supporting substrates with different surface energies. Our results show that the supporting substrates with higher polar surface energy (SiO_2) induces a higher polar surface energy on all graphene samples tested. Further, the polar and dispersive surface energy of graphene varies with the type of functionalization. Physical functionalization, by way of adsorption of VOC, screens the polar interaction potential emanating from the substrate and/or graphene, lowering the polar surface energy. Chemical functionalization, by way of fluorination, has little effect on the polar interaction potential of graphene while dramatically decreasing the dispersive interaction potential, lowering the dispersive surface energy. Chemical functionalization, by way of hydrogenation, has a substrate-dependent effect on the dispersive interaction potential of graphene but dramatically increases the polar interaction potential, raising the polar surface energy on the substrates tested.

Our results provide valuable guidance on how the polarity of monolayer graphene is tuned by chemical functionalization, which has many potential applications. For example, graphene has been used as an atomically thin interface for molecular assembly,[4] hydrophobic and superhydrophobic coatings,[69,70] biosensing,[1−3] and cell adhesion.[17] We expect this knowledge to further inform the rational design of graphene interfaces required for tunable and selective interaction with other molecules.

■ ASSOCIATED CONTENT

Supporting Information

The Supporting Information is available free of charge at https://pubs.acs.org/doi/10.1021/acsami.2c18329.

Surface wettability measurement (S1); extracting surface energies using Fowkes' theory (S2); preparation of graphene samples on SiO_2 and Parylene C (S3); chemical functionalization of graphene (S4); storing the prepared samples in an argon-filled vessel (S5); Raman spectroscopy (S6); X-ray photoelectron spectroscopy (XPS) analysis (S7); and surface topography measurement (S8) (PDF)

■ AUTHOR INFORMATION

Corresponding Authors

Arend van der Zande − *Department of Mechanical Science and Engineering, University of Illinois, Urbana, Illinois 61801, United States; Materials Research Laboratory, University of Illinois, Urbana, Illinois 61801, United States;* orcid.org/0000-0001-5104-9646; Email: arendv@illinois.edu

Nenad Miljkovic − *Department of Mechanical Science and Engineering, University of Illinois, Urbana, Illinois 61801, United States; Materials Research Laboratory and Department of Electrical and Computer Engineering, University of Illinois, Urbana, Illinois 61801, United States; International Institute for Carbon Neutral Energy Research (WPI-I2CNER), Kyushu University, Fukuoka 819-0395, Japan;* orcid.org/0000-0002-0866-3680; Email: nmiljkov@illinois.edu

Authors

James Carpenter − *Department of Mechanical Science and Engineering, University of Illinois, Urbana, Illinois 61801, United States;* orcid.org/0000-0003-1629-0607

Hyunchul Kim − *Department of Mechanical Science and Engineering, University of Illinois, Urbana, Illinois 61801, United States*

Jules Suarez − *Department of Mechanical Science and Engineering, University of Illinois, Urbana, Illinois 61801, United States*

Complete contact information is available at: https://pubs.acs.org/10.1021/acsami.2c18329

Author Contributions

⊥J.C. and H.K. equally contributing authors.

Author Contributions

N.M. and A.v.d.Z. conceived and designed the study. J.C. fabricated the Parylene C substrates. H.K. fabricated the graphene samples on the SiO_2 and Parylene C substrates. J.C. performed contact angle measurements on the samples and subsequent analysis with the help of J.S. and H.K. H.K. conducted the Raman spectroscopy, optical microscopy, and atomic force microscopy of the prepared samples. J.C. designed and benchmarked the pressurized vessel. All authors contributed to the discussion of this work and the writing of the manuscript.

https://doi.org/10.1021/acsami.2c18329
ACS Appl. Mater. Interfaces 2023, 15, 2429−2436

Notes

The authors declare no competing financial interest.

■ ACKNOWLEDGMENTS

This research was primarily supported by the National Science Foundation MRSEC program under NSF Award Number DMR-1720633. N.M. also gratefully acknowledges funding support from the International Institute for Carbon Neutral Energy Research (WPI-I2CNER), sponsored by the Japanese Ministry of Education, Culture, Sports, Science and Technology. J.C. gratefully acknowledges funding support from the I-MRSEC Graduate Fellowship. This work was carried out in part in the Material Research Laboratory Central Facilities, the iMRSEC shared facilities DMR-1720633, and the Micro and Nano Technology Laboratory at the University of Illinois at Urbana-Champaign.

■ REFERENCES

(1) Hwang, M. T.; Heiranian, M.; Kim, Y.; You, S.; Leem, J.; Taqieddin, A.; Faramarzi, V.; Jing, Y.; Park, I.; van der Zande, A. M.; et al. Ultrasensitive Detection of Nucleic Acids Using Deformed Graphene Channel Field Effect Biosensors. *Nat. Commun.* **2020**, *11*, No. 1543.

(2) Syu, Y.-C.; Hsu, W.-E.; Lin, C.-T. Field-Effect Transistor Biosensing: Devices and Clinical Applications. *ECS J. Solid State Sci. Technol.* **2018**, *7*, Q3196.

(3) Wang, W.; Yu, S.; Huang, S.; Bi, S.; Han, H.; Zhang, J.-R.; Lu, Y.; Zhu, J.-J. Bioapplications of DNA Nanotechnology at the Solid−Liquid Interface. *Chem. Soc. Rev.* **2019**, *48*, 4892−4920.

(4) Mali, K. S.; De Feyter, S. Principles of Molecular Assemblies Leading to Molecular Nanostructures. *Philos. Trans. R. Soc., A* **2013**, *371*, No. 20120304.

(5) Suzuki, T. O. D. Intermolecular Energy Transfer at a Solid-Liquid Interface. *Microscale Thermophys. Eng.* **2000**, *4*, 189−196.

(6) Zang, J.; Ryu, S.; Pugno, N.; Wang, Q.; Tu, Q.; Buehler, M. J.; Zhao, X. Multifunctionality and Control of the Crumpling and Unfolding of Large-Area Graphene. *Nat. Mater.* **2013**, *12*, 321−325.

(7) Kireev, D.; Sel, K.; Ibrahim, B.; Kumar, N.; Akbari, A.; Jafari, R.; Akinwande, D. Continuous Cuffless Monitoring of Arterial Blood Pressure Via Graphene Bioimpedance Tattoos. *Nat. Nanotechnol.* **2022**, *17*, 1−7.

(8) Kireev, D.; Brambach, M.; Seyock, S.; Maybeck, V.; Fu, W.; Wolfrum, B.; Offenhäusser, A. Graphene Transistors for Interfacing with Cells: Towards a Deeper Understanding of Liquid Gating and Sensitivity. *Sci. Rep.* **2017**, *7*, No. 6658.

(9) Kempaiah, R.; Chung, A.; Maheshwari, V. Graphene as Cellular Interface: Electromechanical Coupling with Cells. *ACS Nano* **2011**, *5*, 6025−6031.

(10) Sitsanidis, E. D.; Schirmer, J.; Lampinen, A.; Mentel, K. K.; Hiltunen, V.-M.; Ruokolainen, V.; Johansson, A.; Myllyperkiö, P.; Nissinen, M.; Pettersson, M. Tuning Protein Adsorption on Graphene Surfaces Via Laser-Induced Oxidation. *Nanoscale Adv.* **2021**, *3*, 2065−2074.

(11) Zhou, K.; Chen, J.; Wang, T.; Su, Y.; Qiao, L.; Yan, Y. Effect of Surface Energy on Protein Adsorption Behaviours of Treated Cocrmo Alloy Surfaces. *Appl. Surf. Sci.* **2020**, *520*, No. 146354.

(12) Baszkin, A.; Lyman, D. J. The Interaction of Plasma Proteins with Polymers. I. Relationship between Polymer Surface Energy and Protein Adsorption/Desorption. *J. Biomed. Mater. Res.* **1980**, *14*, 393−403.

(13) Wang, Y.; Lee, W. C.; Manga, K. K.; Ang, P. K.; Lu, J.; Liu, Y. P.; Lim, C. T.; Loh, K. P. Fluorinated Graphene for Promoting Neuro-Induction of Stem Cells. *Adv. Mater.* **2012**, *24*, 4285−4290.

(14) Hallab, N. J.; Bundy, K. J.; O'Connor, K.; Moses, R. L.; Jacobs, J. J. Evaluation of Metallic and Polymeric Biomaterial Surface Energy and Surface Roughness Characteristics for Directed Cell Adhesion. *Tissue Eng.* **2001**, *7*, 55−71.

(15) Elias, D. C.; Nair, R. R.; Mohiuddin, T. M. G.; Morozov, S. V.; Blake, P.; Halsall, M. P.; Ferrari, A. C.; Boukhvalov, D. W.; Katsnelson, M. I.; Geim, A. K.; Novoselov, K. S. Control of Graphene's Properties by Reversible Hydrogenation: Evidence for Graphane. *Science* **2009**, *323*, 610−613.

(16) Balog, R.; Jørgensen, B.; Nilsson, L.; Andersen, M.; Rienks, E.; Bianchi, M.; Fanetti, M.; Lægsgaard, E.; Baraldi, A.; Lizzit, S.; Sljivancanin, Z.; Besenbacher, F.; Hammer, B.; Pedersen, T. G.; Hofmann, P.; Hornekær, L. Bandgap Opening in Graphene Induced by Patterned Hydrogen Adsorption. *Nat. Mater.* **2010**, *9*, 315−319.

(17) Son, J.; Lee, J.-Y.; Han, N.; Cha, J.; Choi, J.; Kwon, J.; Nam, S.; Yoo, K.-H.; Lee, G.-H.; Hong, J. Tunable Wettability of Graphene through Nondestructive Hydrogenation and Wettability-Based Patterning for Bioapplications. *Nano Lett.* **2020**, *20*, 5625−5631.

(18) Robinson, J. T.; Burgess, J. S.; Junkermeier, C. E.; Badescu, S. C.; Reinecke, T. L.; Perkins, F. K.; Zalalutdniov, M. K.; Baldwin, J. W.; Culbertson, J. C.; Sheehan, P. E.; Snow, E. S. Properties of Fluorinated Graphene Films. *Nano Lett.* **2010**, *10*, 3001−3005.

(19) Nair, R. R.; Ren, W.; Jalil, R.; Riaz, I.; Kravets, V. G.; Britnell, L.; Blake, P.; Schedin, F.; Mayorov, A. S.; Yuan, S.; Katsnelson, M. I.; Cheng, H. M.; Strupinski, W.; Bulusheva, L. G.; Okotrub, A. V.; Grigorieva, I. V.; Grigorenko, A. N.; Novoselov, K. S.; Geim, A. K. Fluorographene: A Two-Dimensional Counterpart of Teflon. *Small* **2010**, *6*, 2877−2884.

(20) Feng, W.; Long, P.; Feng, Y.; Li, Y. Two-Dimensional Fluorinated Graphene: Synthesis, Structures, Properties and Applications. *Adv. Sci.* **2016**, *3*, No. 1500413.

(21) Son, J.; Buzov, N.; Chen, S.; Sung, D.; Ryu, H.; Kwon, J.; Kim, S.; Namiki, S.; Xu, J.; Hong, S.; Watanabe, K.; Taniguchi, T.; King, W. P.; Lee, G. H.; Zande, A. M. v. d. Tailoring Surface Properties Via Functionalized Hydrofluorinated Graphene Compounds. *Adv. Mater.* **2019**, *31*, No. 1903424.

(22) Vervuurt, R. H. J.; Karasulu, B.; Verheijen, M. A.; Kessels, W. M.; Bol, A. A. Uniform Atomic Layer Deposition of Al2o3 on Graphene by Reversible Hydrogen Plasma Functionalization. *Chem. Mater.* **2017**, *29*, 2090−2100.

(23) Lee, W.-K.; Hernández, S. C.; Robinson, J. T.; Walton, S. G.; Sheehan, P. E. Fluorinated Graphene Enables the Growth of Inorganic Thin Films by Chemical Bath Deposition on Otherwise Inert Substrates. *ACS Appl. Mater. Interfaces* **2017**, *9*, 677−683.

(24) Wheeler, V.; Garces, N.; Nyakiti, L.; Myers-Ward, R.; Jernigan, G.; Culbertson, J.; Eddy, C.; Kurt Gaskill, D. Fluorine Functionalization of Epitaxial Graphene for Uniform Deposition of Thin High-K Dielectrics. *Carbon* **2012**, *50*, 2307−2314.

(25) Rodríguez González, M. C.; Leonhardt, A.; Stadler, H.; Eyley, S.; Thielemans, W.; De Gendt, S.; Mali, K. S.; De Feyter, S. Multicomponent Covalent Chemical Patterning of Graphene. *ACS Nano* **2021**, *15*, 10618−10627.

(26) Son, J.; Cha, J.; Hong, J. Electrical Patterning of Graphene Circuitry by Hydrogenation for Transparent and Flexible Devices. *Chem. Mater.* **2021**, *33*, 574−579.

(27) Son, J.; Ryu, H.; Kwon, J.; Huang, S.; Yu, J.; Xu, J.; Watanabe, K.; Taniguchi, T.; Ji, E.; Lee, S.; Shin, Y.; Kim, J. H.; Kim, K.; Zande, A. M. v. d.; Lee, G.-H. Tailoring Single- and Double-Sided Fluorination of Bilayer Graphene Via Substrate Interactions. *Nano Lett.* **2021**, *21*, 891−898.

(28) Shih, C.-J.; Wang, Q. H.; Lin, S.; Park, K.-C.; Jin, Z.; Strano, M. S.; Blankschtein, D. Breakdown in the Wetting Transparency of Graphene. *Phys. Rev. Lett.* **2012**, *109*, No. 176101.

(29) Shih, C.-J.; Strano, M. S.; Blankschtein, D. Wetting Translucency of Graphene. *Nat. Mater.* **2013**, *12*, 866−869.

(30) Rafiee, J.; Mi, X.; Gullapalli, H.; Thomas, A. V.; Yavari, F.; Shi, Y.; Ajayan, P. M.; Koratkar, N. A. Wetting Transparency of Graphene. *Nat. Mater.* **2012**, *11*, 217−222.

(31) Presel, F.; Gijon, A.; Hernández, E. R.; Lacovig, P.; Lizzit, S.; Alfe, D.; Baraldi, A. Translucency of Graphene to Van Der Waals Forces Applies to Atoms/Molecules with Different Polar Character. *ACS Nano* **2019**, *13*, 12230−12241.

https://doi.org/10.1021/acsami.2c18329
ACS Appl. Mater. Interfaces 2023, 15, 2429−2436

(32) Miller, W. J.; Abbott, N. L. Influence of Van Der Waals Forces from Metallic Substrates on Fluids Supported on Self-Assembled Monolayers Formed from Alkanethiols. *Langmuir* **1997**, *13*, 7106−7114.
(33) Yan, X.; Huang, Z.; Sett, S.; Oh, J.; Cha, H.; Li, L.; Feng, L.; Wu, Y.; Zhao, C.; Orejon, D.; Chen, F.; Miljkovic, N. Atmosphere-Mediated Superhydrophobicity of Rationally Designed Micro/Nanostructured Surfaces. *ACS Nano* **2019**, *13*, 4160−4173.
(34) Oh, J.; Orejon, D.; Park, W.; Cha, H.; Sett, S.; Yokoyama, Y.; Thoreton, V.; Takata, Y.; Miljkovic, N. The Apparent Surface Free Energy of Rare Earth Oxides Is Governed by Hydrocarbon Adsorption. *iScience* **2021**, *25*, No. 103691.
(35) Preston, D. J.; Miljkovic, N.; Sack, J.; Enright, R.; Queeney, J.; Wang, E. N. Effect of Hydrocarbon Adsorption on the Wettability of Rare Earth Oxide Ceramics. *Appl. Phys. Lett.* **2014**, *105*, No. 011601.
(36) Lundy, R.; Byrne, C.; Bogan, J.; Nolan, K.; Collins, M. N.; Dalton, E.; Enright, R. Exploring the Role of Adsorption and Surface State on the Hydrophobicity of Rare Earth Oxides. *ACS Appl. Mater. Interfaces* **2017**, *9*, 13751−13760.
(37) Liu, Z.; Song, Y.; Rajappan, A.; Wang, E. N.; Preston, D. J. Temporal Evolution of Surface Contamination under Ultra-High Vacuum. *Langmuir* **2022**, *38*, 1252−1258.
(38) Kozbial, A.; Li, Z.; Sun, J.; Gong, X.; Zhou, F.; Wang, Y.; Xu, H.; Liu, H.; Li, L. Understanding the Intrinsic Water Wettability of Graphite. *Carbon* **2014**, *74*, 218−225.
(39) Aria, A. I.; Kidambi, P. R.; Weatherup, R. S.; Xiao, L.; Williams, J. A.; Hofmann, S. Time Evolution of the Wettability of Supported Graphene under Ambient Air Exposure. *J. Phys. Chem. C* **2016**, *120*, 2215−2224.
(40) Kozbial, A.; Li, Z.; Conaway, C.; McGinley, R.; Dhingra, S.; Vahdat, V.; Zhou, F.; D'Urso, B.; Liu, H.; Li, L. Study on the Surface Energy of Graphene by Contact Angle Measurements. *Langmuir* **2014**, *30*, 8598−8606.
(41) Costa, M. C. F.; Parra, G. G.; Larrude, D. R.; Fechine, G. J. Screening Effect of Cvd Graphene on the Surface Free Energy of Substrates. *Phys. Chem. Chem. Phys.* **2020**, *22*, 16672−16680.
(42) Wang, S.; Zhang, Y.; Abidi, N.; Cabrales, L. Wettability and Surface Free Energy of Graphene Films. *Langmuir* **2009**, *25*, 11078−11081.
(43) Raj, R.; Maroo, S. C.; Wang, E. N. Wettability of Graphene. *Nano Lett.* **2013**, *13*, 1509−1515.
(44) Hong, G.; Han, Y.; Schutzius, T. M.; Wang, Y.; Pan, Y.; Hu, M.; Jie, J.; Sharma, C. S.; Müller, U.; Poulikakos, D. On the Mechanism of Hydrophilicity of Graphene. *Nano Lett.* **2016**, *16*, 4447−4453.
(45) Kozbial, A.; Zhou, F.; Li, Z.; Liu, H.; Li, L. Are Graphitic Surfaces Hydrophobic? *Acc. Chem. Res.* **2016**, *49*, 2765−2773.
(46) Prydatko, A. V.; Belyaeva, L. A.; Jiang, L.; Lima, L. M. C.; Schneider, G. F. Contact Angle Measurement of Free-Standing Square-Millimeter Single-Layer Graphene. *Nat. Commun.* **2018**, *9*, No. 4185.
(47) Sharma, P. K.; Rao, K. H. Analysis of Different Approaches for Evaluation of Surface Energy of Microbial Cells by Contact Angle Goniometry. *Adv. Colloid Interface Sci.* **2002**, *98*, 341−463.
(48) Fowkes, F. M. Additivity of Intermolecular Forces at Interfaces. I. Determination of the Contribution to Surface and Interfacial Tensions of Dispersion Forces in Various Liquids. *J. Phys. Chem. A* **1963**, *67*, 2538−2541.
(49) Chen, Y.; Gong, X. L.; Gai, J. G. Progress and Challenges in Transfer of Large-Area Graphene Films. *Adv. Sci.* **2016**, *3*, No. 1500343.
(50) Gupta, P.; Dongare, P. D.; Grover, S.; Dubey, S.; Mamgain, H.; Bhattacharya, A.; Deshmukh, M. M. A Facile Process for Soak-and-Peel Delamination of Cvd Graphene from Substrates Using Water. *Sci. Rep.* **2014**, *4*, No. 3882.
(51) Diankov, G.; Neumann, M.; Goldhaber-Gordon, D. Extreme Monolayer-Selectivity of Hydrogen-Plasma Reactions with Graphene. *ACS Nano* **2013**, *7*, 1324−1332.
(52) Stine, R.; Lee, W.-K.; Whitener, K. E.; Robinson, J. T.; Sheehan, P. E. Chemical Stability of Graphene Fluoride Produced by Exposure to Xef 2. *Nano Lett.* **2013**, *13*, 4311−4316.
(53) Ferrari, A. C.; Robertson, J. Interpretation of Raman Spectra of Disordered and Amorphous Carbon. *Phys. Rev. B* **2000**, *61*, 14095.
(54) Ferrari, A. C.; Basko, D. M. Raman Spectroscopy as a Versatile Tool for Studying the Properties of Graphene. *Nat. Nanotechnol.* **2013**, *8*, 235−246.
(55) Hong, J.; Park, M. K.; Lee, E. J.; Lee, D.; Hwang, D. S.; Ryu, S. Origin of New Broad Raman D and G Peaks in Annealed Graphene. *Sci. Rep.* **2013**, *3*, No. 2700.
(56) Son, J.; Lee, S.; Kim, S. J.; Park, B. C.; Lee, H.-K.; Kim, S.; Kim, J. H.; Hong, B. H.; Hong, J. Hydrogenated Monolayer Graphene with Reversible and Tunable Wide Band Gap and Its Field-Effect Transistor. *Nat. Commun.* **2016**, *7*, No. 13261.
(57) Li, Z.; Wang, Y.; Kozbial, A.; Shenoy, G.; Zhou, F.; McGinley, R.; Ireland, P.; Morganstein, B.; Kunkel, A.; Surwade, S. P.; Li, L.; Liu, H. Effect of Airborne Contaminants on the Wettability of Supported Graphene and Graphite. *Nat. Mater.* **2013**, *12*, 925−931.
(58) Israelachvilli, J. N. *Intermolecular and Surface Forces*; Academic Press, 2011.
(59) Correia, N. T.; Ramos, J. J. M.; Saramago, B. J. V.; Calado, J. C. G. Estimation of the Surface Tension of a Solid: Application to a Liquid Crystalline Polymer. *J. Colloid Interface Sci.* **1997**, *189*, 361−369.
(60) Bagheri, M. H.; Loibl, R. T.; Boscoboinik, J. A.; Schiffres, S. N. Adsorption Transparency of Supported Graphene. *Carbon* **2019**, *155*, 580−586.
(61) Tachikawa, H.; Kawabata, H. Additions of Fluorine Atoms to the Surfaces of Graphene Nanoflakes: A Density Functional Theory Study. *Solid State Sci.* **2019**, *97*, No. 106007.
(62) Mayrhofer, L.; Moras, G.; Mulakaluri, N.; Rajagopalan, S.; Stevens, P. A.; Moseler, M. Fluorine-Terminated Diamond Surfaces as Dense Dipole Lattices: The Electrostatic Origin of Polar Hydrophobicity. *J. Am. Chem. Soc.* **2016**, *138*, 4018−4028.
(63) Lemal, D. M. Perspective on Fluorocarbon Chemistry. *J. Org. Chem.* **2004**, *69*, 1−11.
(64) Giovambattista, N.; Debenedetti, P. G.; Rossky, P. J. Enhanced Surface Hydrophobicity by Coupling of Surface Polarity and Topography. *Proc. Natl. Acad. Sci.* **2009**, *106*, 15181−15185.
(65) Dalvi, V. H.; Rossky, P. J. Molecular Origins of Fluorocarbon Hydrophobicity. *Proc. Natl. Acad. Sci.* **2010**, *107*, 13603−13607.
(66) Hu, S.; Lozada-Hidalgo, M.; Wang, F. C.; Mishchenko, A.; Schedin, F.; Nair, R. R.; Hill, E. W.; Boukhvalov, D. W.; Katsnelson, M. I.; Dryfe, R. A. W.; Grigorieva, I. V.; Wu, H. A.; Geim, A. K. Proton Transport through One-Atom-Thick Crystals. *Nature* **2014**, *516*, 227−230.
(67) Lozada-Hidalgo, M.; Hu, S.; Marshall, O.; Mishchenko, A.; Grigorenko, A. N.; Dryfe, R. A. W.; Radha, B.; Grigorieva, I. V.; Geim, A. K. Sieving Hydrogen Isotopes through Two-Dimensional Crystals. *Science* **2016**, *351*, 68−70.
(68) Sun, P. Z.; Yang, Q.; Kuang, W. J.; Stebunov, Y. V.; Xiong, W. Q.; Yu, J.; Nair, R. R.; Katsnelson, M. I.; Yuan, S. J.; Grigorieva, I. V.; Lozada-Hidalgo, M.; Wang, F. C.; Geim, A. K. Limits on Gas Impermeability of Graphene. *Nature* **2020**, *579*, 229−232.
(69) Preston, D. J.; Mafra, D. L.; Miljkovic, N.; Kong, J.; Wang, E. N. Scalable Graphene Coatings for Enhanced Condensation Heat Transfer. *Nano Lett.* **2015**, *15*, 2902−2909.
(70) Jiang, H.-B.; Zhang, Y.-L.; Han, D.-D.; Xia, H.; Feng, J.; Chen, Q.-D.; Hong, Z.-R.; Sun, H.-B. Bioinspired Fabrication of Superhydrophobic Graphene Films by Two-Beam Laser Interference. *Adv. Funct. Mater.* **2014**, *24*, 4595−4602.

https://doi.org/10.1021/acsami.2c18329
ACS Appl. Mater. Interfaces 2023, 15, 2429−2436